Full Length Article

Dual MPPT algorithm for dual PV source fed Open-End Winding Induction Motor Drive for pumping application

CrossMark

Sachin Jain [a], Chinthamalla Ramulu [a], Sanjeevikumar Padmanaban [b,*], Joseph Olorunfemi Ojo [c,d], Ahmet H. Ertas [e]

[a] Department of Electrical Engineering, National Institute of Technology, Warangal, Telangana 506004, India
[b] Department of Electrical and Electronics Engineering, University of Johannesburg, Auckland Park, South Africa
[c] Center for Energy System Research, Department of Electrical & Computer Engineering, Tennessee Technological University, Cookeville, 38505-Tennessee, United States
[d] Eskom Centre of Excellence in HVDC Engineering, University of KwaZulu-Natal, Durban, South Africa
[e] Department of Biomedical Engineering, Engineering Faculty, Karabuk University, Turkey

ARTICLE INFO

ABSTRACT

This paper presents a single-stage solution for a dual Maximum Power Point Tracking (MPPT) technique for a solar Photovoltaic (PV) fed water pumping system. The proposed solar PV fed pumping system uses a three-phase Open-End Winding Induction Motor (OEWIM) coupled to a centrifugal water pump. The OEWIM is connected via two time tested two-level three-phase inverters powered by two independent solar PV arrays. These two PV arrays can be configured independently and the employed dual MPPT algorithm operate the two PV sources at or near maximum power point (MPP) irrespective of its configuration. Usage of different array configurations may help in attaining more number of levels (greater than or equals to three) in the inverter output voltage (OEWIM phase voltage). Furthermore, the system is operated using decoupled Pulse Width Modulation (PWM) technique with V/f control along with the proposed dual MPPT technique. The maximum power extracted by the dual MPPT algorithm from two PV sources is optimally utilized by the OEWIM. This can be supported by the low slip value at all the operating conditions. The detailed analysis of proposed system and the simulation results are presented.

1. Introduction

Today to meet the never ending and increasing demand of electrical energy, most of the research is diverted towards the utilization of renewable sources such as solar PhotoVoltaic (PV), wind, fuel cells, thermo-generator etc. Among these sources, solar PV technology is considered as the most viable solution to meet the electrical energy demand. Noiseless operation, low maintenance and zero pollution further adds to the popularity of solar PV source, which directly converts the solar energy into the electrical energy. The solar PV system can be used either in electric power grid-tied mode or in the stand-alone mode. In grid-tied application [1–3] the PV source feeds the high quality ac power into the grid. Whereas in stand-alone systems, the generated PV power could drive the stand-alone loads [4–8] like water pumps, air compressors, household etc using additional power sources like battery, fuel cell etc.

However, for stand-alone loads like solar fed water pumping applications [7,8] used in agriculture, industries, hydro power plant and residential buildings gives the option of storing solar PV energy without using additional power sources. The solar PV energy can be stored in the form of potential energy by storing water in the tank [9], dam etc at the required height above ground level. The stored energy or water, then can be utilized with respect to demand or requirement. Thus, in such systems additional power sources for storing the electrical energy may not be required and it also gives the option of continuously operating solar PV array at or near MPP. Thus, the system effectively utilizes the solar PV power for all the environmental conditions. Some of the solutions for the PV fed water pumping systems were introduced since 1980s, where a dc motor coupled to a centrifugal pump is directly powered from the PV source [10–12] and with a converter for MPP tracking [13]. The use of dc motor may be overruled because of its high cost and continuous maintenance [14]. The other option to replace a dc motor could be the brushless dc (BLDC) motor [15,16]. Presently, the use of BLDC motor in a PV pumping system may not be a feasible solution because of its high cost and the requirement of complex control circuitry. So, the use of 3-Φ,

* Corresponding author.
 E-mail address: sanjeevi_12@yahoo.co.in (S. Padmanaban).
 Peer review under responsibility of Karabuk University.

induction motor could be a feasible and better solution for PV fed water pumping system.

The use of 3-Φ induction motor in the PV fed water pumping system has been reported in the literature [17–19]. Most of the research work includes the use of conventional induction motor with the two or single power conversion stage. The two-stage system [20–22] includes a dc–dc converter and an inverter in between the solar PV source and the induction motor as shown in Fig. 1(a). The dc-dc converter in two-stage PV system is used to boost the voltage and helps in tracking maximum power from the PV source. And the inverter is used to provide the required ac power to the motor-pump load. The other solution includes the single-stage system [23–28] where a single inverter is used as shown in Fig. 1(b). It is an integrated solution in which the Maximum Power point Tracking (MPPT) and motor control, both are governed by a single inverter.

Most recently, the advantage of a single-stage system along with the benefits of Open-End Winding Induction Motor (OEWIM) [29–35] is incorporated in a PV pumping system and the work is reported in [26,27]. The given solution uses a single solar PV array to drive OEWIM through the dual-inverter giving only three-level output as shown in Fig. 1(c). Also, the usage of single PV array increases the risk of shading issues in the PV array configuration. This risk/probability of shading in the PV array increases with the increase in the size or power rating of the PV array. Further, the operation under partially shaded condition deteriorates the performance of the PV system. This is because of the presence of multiple local peaks and a global peak in the p–v (power versus voltage) characteristics of the PV array. The presence of local peaks

in the p–v characteristic affects the performance of the MPPT algorithm which further effects the overall performance of the system. Further, there is no option for dual or multiple configurations for PV arrays to minimize shading problem. One solution could be the usage of dual or distributed Maximum Power Point Tracking (MPPT) [36–42] at dc–dc converter stage in case 2-stage system. However, this would increase the cost and complexity of the system with the increased number of dc–dc converters. Thus, there is a need for the single-stage system with simple control which has the option of dual or distributed MPPT.

Thus, it is apparent that there is a need for low cost, high performance single-stage low PV array voltage water pumping system with dual/distributed solar PV arrays arrangement for minimizing effect of shading problem. It should also have three or more number of levels in the phase voltage, wide band-width of PV source operating voltage and should have the option of dual/distributed MPPT. This paper introduces a PV pumping system which uses OEWIM-pump powered by two electrically isolated PV sources through two two-level inverters as shown in Fig. 1(d). The OEWIM with two two-level inverters provide the three-level output voltage which improves the system performance when compared to conventional two-level solutions in terms of torque ripple, power ripple etc. Also, the number of levels in the output voltage can be more than three if the asymmetrical PV array configurations are utilized i.e., by using solar PV arrays with different size or power ratings.

Most importantly, the implementation of dual/distributed MPPT algorithm (limited to dual MPPT in this case) is made possible with the proposed system for PV pumping application. The dual
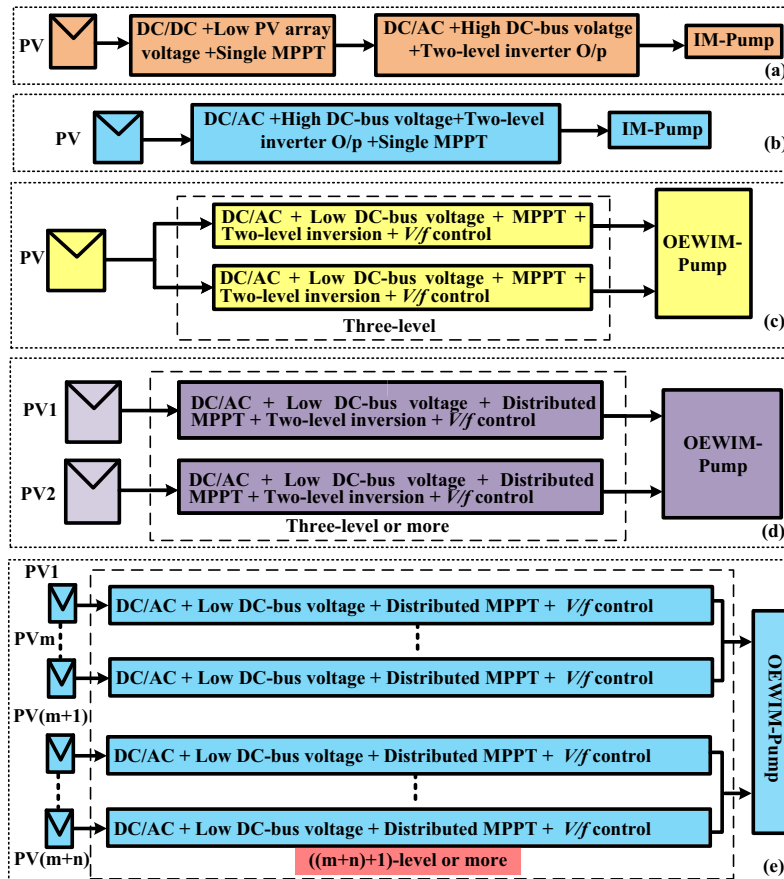

Fig. 1. Block diagram of (a) two-stage single PV source powered centrifugal water pump (b) single-stage single PV source powered centrifugal water pump (c) single-stage single PV source powered OEWIM-pump (d) proposed single-stage dual PV source powered OEWIM-pump drive with dual MPPT (e) extended version for (d).

MPPT helps in the effective tracking of maximum power from both the PV sources separately. Furthermore, the proposed configuration can be extended to have multiple PV sources (*m+n*) as shown in Fig. 1(e) with distributed MPPT technique given by Sonti et al. [42]. This helps in the generation of '*m+n+1*' or higher number of levels in the output voltage [43]. However, the work presented in this manuscript is limited to the basic two isolated solar PV sources.

Rest of the paper is organized as follows. In Section 2, the mathematical modeling of all the major equipment used in the proposed system is described. Section 3 consists of the detailed operation and control strategy used for the proposed system. Simulation results are presented in Section 4, whereas the fifth section concludes the paper.

2. Modeling of the proposed system

The circuit schematic for the proposed system is shown in Fig. 2. It consists of two sets of PV array. Each PV array power is conditioned by their respective inverter connected to them. The two inverters independently condition the PV power using their respective MPPT algorithm's. Thus, both the inverters operate their PV sources at or near MPPT. The extracted power from both the PV sources is then used by the OEWIM-pump. The mathematical model of PV array, dual-inverter and the OEWIM-pump used in the simulation along with the analysis of the proposed system are described in the following sub-sections.

2.1. Solar PV array model

The mathematical model of PV cell is described by the *i–v* (current versus voltage) characteristic equation of the basic PV cell unit. The *i–v* characteristic equation [44] of the PV cell is given by,

$$i_{pv} = i_L - i_o\left(e^{\frac{q(v_{pv}+i_{pv}R_s)}{AkT}} - 1\right) \tag{1}$$

where 'i_{pv}' corresponds to the PV cell current, 'i_L' is the generated photo-current, 'i_o' corresponds to the diode reverse saturation current, 'A' is the diode ideality factor, 'k' is the Boltzmann constant,

'q' is the electron charge, 'T' is the PV cell operating temperature, 'R_s' is the PV cell series parasitic resistance, and 'v_{pv}' is the PV cell voltage.

The given *i–v* characteristic equation is then modified with respect to the series–parallel arrangements of the cells for the PV array configuration used in the system. The two PV arrays PV1 and PV2 are individually connected to Inverter-1 and Inverter-2 respectively through the PV/dc-bus capacitor 'C_{pv}' as shown in Fig. 2. Now, applying KCL at nodal points 'n1' and 'n2' of Inverter-1 and Inverter-2 respectively (Fig. 2) we have,

$$i_{pv1} = C_{pv}\frac{dv_{pv1}}{dt} + i_{inv1} \tag{2}$$

$$i_{pv2} = C_{pv}\frac{dv_{pv2}}{dt} + i_{inv2} \tag{3}$$

where 'v_{pv1}' and 'v_{pv2}' are the PV/dc-bus voltage for PV arrays PV1 and PV2, respectively; 'i_{pv1}' and 'i_{pv2}' are the currents generated by the PV arrays PV1 and PV2 respectively. Further, 'i_{inv1}' and 'i_{inv2}' are the dc-bus current drawn by Inverter-1 and Inverter-2 respectively.

2.2. Three-level isolated dual-inverter model

Mathematical model for the electrically isolated dual-inverter (Inverter-1 and Inverter-2) is derived using switching functions. The switching function, Sw_j (where $j \in \{a1, b1, c1\}$ for Inverter-1 and $\{a2, b2, c2\}$ for Inverter-2) hold the values 1 or −1, depending on top or bottom switch of leg 'j' in corresponding inverter is turned ON respectively. Using the magnitude of dc-bus voltage and switching function 'Sw_j' the pole voltage at respective leg of inverter can be derived. For this a hypothetical ground point 'o' and 'o''' for Inverter-1 and Inverter-2 respectively are assumed as shown in Fig. 2. This simplifies the calculation of pole voltage at output terminals for both the inverters. Thus, pole voltage 'v_{a1o}' at terminal 'a1' of Inverter-1 can be written as,

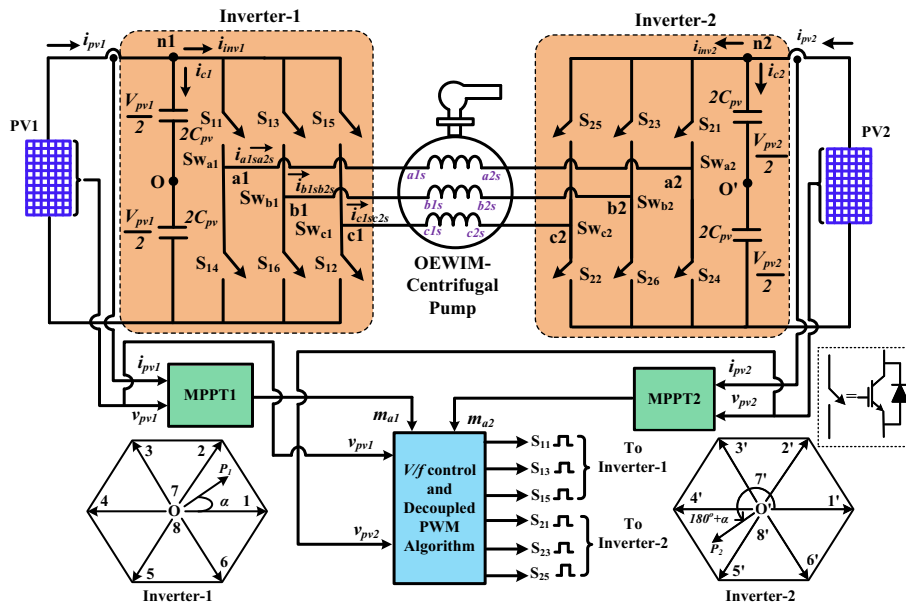$$v_{a1o} = Sw_{a1}\left(\frac{V_{pv1}}{2}\right) \tag{4}$$

Fig. 2. Schematic circuit diagram of the proposed system.

Similarly, the pole voltages 'v_{jo}' for Inverter-1 and 'v_{jo}' for Inverter-2 can be derived for both the inverters. Once the pole voltages are known, the common mode voltage of the Inverter-1 (v_{on}) and Inverter-2 ($v_{o'n}$) are given by,

$$v_{on} = \frac{1}{3}(v_{a1o} + v_{b1o} + v_{c1o}) \tag{5}$$

$$v_{o'n} = \frac{1}{3}(v_{a2o'} + v_{b2o'} + v_{c2o'}) \tag{6}$$

where 'n' represents a hypothetical ground point of the OEWIM. Now, using pole voltage and common mode voltage, the voltage 'v_{a1a2}' between terminals '$a1$' and '$a2$' can be calculated as,

$$v_{a1a2} = \frac{V_{pv1}}{2}\left\{\left(\frac{2}{3}\right)Sw_{a1} - \frac{1}{3}(Sw_{b1} + Sw_{c1})\right\}$$
$$- \frac{V_{pv2}}{2}\left\{\left(\frac{2}{3}\right)Sw_{a2} - \frac{1}{3}(Sw_{b2} + Sw_{c2})\right\} \tag{7}$$

This also represents the stator phase voltage 'v_{a1sa2s}' of OEWIM at phase '$a1sa2s$' (see Fig. 3). Similarly, the other stator phase voltages 'v_{b1sb2s}' and 'v_{c1sc2s}' of the OEWIM at '$b1sb2s$' and '$c1sc2s$' respectively can be derived. Once the phase voltages applied to OEWIM are known, then the respective phase currents 'i_{a1sa2s}', 'i_{b1sb2s}' and 'i_{c1sc2s}' can be calculated using motor dynamic model as described in the next sub-section. The derived phase currents can be used for the calculation of the inverter current 'i_{inv1}' and 'i_{inv2}' of both Inverter-1 and Inverter-2 respectively, as given below,

$$i_{inv1} = \frac{1}{2}(Sw_{a1} + 1)(i_{a1sa2s}) + \frac{1}{2}(Sw_{b1} + 1)(i_{b1sb2s}) + \frac{1}{2}(Sw_{c1} + 1)(i_{c1sc2s}) \tag{8}$$

$$i_{inv2} = \frac{1}{2}(Sw_{a2} + 1)(-i_{a1sa2s}) + \frac{1}{2}(Sw_{b2} + 1)(-i_{b1sb2s}) + \frac{1}{2}(Sw_{c2} + 1)(-i_{c1sc2s}) \tag{9}$$

2.3. Open-End Winding Induction Motor Model

An OEWIM can be realized physically by avoiding the shorting of stator windings [45]. This facilitates to have six stator terminals namely '$a1s$', '$a2s$', '$b1s$', '$b2s$', '$c1s$' and '$c2s$' as shown in Fig. 3. The rotor winding is shorted and unaltered which is represented by 'ar', 'br' and 'cr' axes. The rotor is displaced with the stator by an angle 'δ_r' with respect to '$a1s$' reference axis as depicted in Fig. 3. The phase voltage applied to the OEWIM stator can be expressed as,
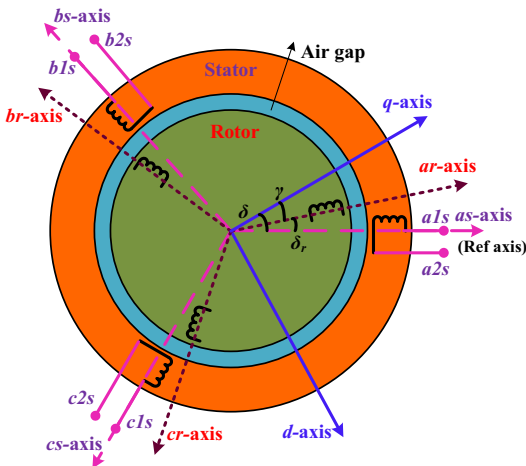

Fig. 3. The machine model of OEWIM [26].

$$\begin{bmatrix} v_{a1sa2s} \\ v_{b1sb2s} \\ v_{c1sc2s} \end{bmatrix} = \begin{bmatrix} r_s & 0 & 0 \\ 0 & r_s & 0 \\ 0 & 0 & r_s \end{bmatrix}\begin{bmatrix} i_{a1sa2s} \\ i_{b1sb2s} \\ i_{c1sc2s} \end{bmatrix} + p\begin{bmatrix} \lambda_{a1sa2s} \\ \lambda_{b1sb2s} \\ \lambda_{c1sc2s} \end{bmatrix} \tag{10}$$

where 'λ_{a1sa2s}', 'λ_{b1sb2s}', and 'λ_{c1sc2s}' are the flux-linkage for respective stator phase windings of the motor; 'r_s' is the per phase stator winding resistance.

The three-phase stator voltages can be mapped into the d–q space using power invariant transformation given below:

$$\begin{bmatrix} v_q \\ v_d \\ v_o \end{bmatrix} = \frac{2}{3}\begin{bmatrix} \cos\varphi & \cos(\varphi - 2\pi/3) & \cos(\varphi + 2\pi/3) \\ \sin\varphi & \sin(\varphi - 2\pi/3) & \sin(\varphi + 2\pi/3) \\ 1/2 & 1/2 & 1/2 \end{bmatrix}\begin{bmatrix} v_{a1sa2s} \\ v_{b1sb2s} \\ v_{c1sc2s} \end{bmatrix} \tag{11}$$

where 'q' is the quadrature axis quantity, 'd' is the direct axis quantity, the angle ϕ = 'δ' for stator transformation and 'γ' for rotor transformation. From Fig. 3, 'δ' is the angle between stator '$a1s$' axis and q-axis, 'γ' is the angle between rotor 'ar' axis and q-axis, or otherwise $\gamma = \delta - \delta_r$. The voltage equations for dynamic model of OEWIM can be expressed as,

$$v_{qs} = i_{qs}r_s + \omega\lambda_{ds} + \frac{d\lambda_{qs}}{dt} \tag{12}$$

$$v'_{qr} = i'_{qr}r'_r + (\omega - \omega_r)\lambda'_{dr} + \frac{d\lambda'_{qr}}{dt} \tag{13}$$

$$v_{ds} = i_{ds}r_s - \omega\lambda_{qs} + \frac{d\lambda_{ds}}{dt} \tag{14}$$

$$v'_{dr} = i'_{dr}r'_r - (\omega - \omega_r)\lambda'_{qr} + \frac{d\lambda'_{dr}}{dt} \tag{15}$$

where " ' " represent rotor side quantities referred to stator, 'ω' is the synchronous speed, 'ω_r' is the rotor speed or instantaneous angular velocity of the motor shaft (rad/s). Here 'v'_{qr}', 'v'_{dr}' are equal to zero, since a squirrel cage induction motor is considered for simulation, in which rotor terminals are shorted. Now the equations for flux-linkage for OWEIM are given by,

$$\begin{pmatrix} \lambda_{qs} \\ \lambda_{ds} \\ \lambda'_{qr} \\ \lambda'_{dr} \end{pmatrix} = \begin{pmatrix} L_m + L_{ls} & 0 & L_m & 0 \\ 0 & L_m + L_{ls} & 0 & L_m \\ L_m & 0 & L_m + L'_{lr} & 0 \\ 0 & L_m & 0 & L_m + L'_{lr} \end{pmatrix}\begin{pmatrix} i_{qs} \\ i_{ds} \\ i'_{qr} \\ i'_{dr} \end{pmatrix} \tag{16}$$

where, 'L_m', 'L_{ls}' and '$L_r^{\square}$' are the magnetizing inductance, leakage inductance of stator winding and leakage inductance of rotor winding referred to stator respectively.

The electromagnetic torque 'm_d' developed in the OEWIM is expressed as

$$m_d = \frac{3}{2}\frac{p}{2}\frac{L_m}{L_s}(\lambda_{qs}i'_{dr} - \lambda_{ds}i'_{qr}) \tag{17}$$

where 'p' is the number of poles of the machine.

The mechanical equation governing the OEWIM-pump drive is expressed as

$$J\frac{d\omega_r}{dt} + B\omega_r + m_L = m_d \tag{18}$$

where 'J' is the moment of inertia for OEWIM (kg-m^2), 'B' is the coefficient of centrifugal load torque, 'm_L' is the centrifugal pump load torque given by,

$$m_L = K_w\omega_r^2 \tag{19}$$

where 'K_w' is the centrifugal pump constant.

3. Operation and control strategy used for the proposed system

The proposed system uses dual MPPT algorithm which is assimilated with the decoupled PWM technique along with V/f control. Since, the proposed system uses two isolated PV sources, the generated maximum power from these sources can be extracted separately using two independent MPPT algorithms (dual MPPT). As the proposed system is a single-stage and uses two independent MPPT algorithms, there is a challenge involved in the assimilation of the dual MPPT algorithm along with the motor control. The dual MPPT algorithm generates two different values of modulation indices 'm_{a1}' and 'm_{a2}' for both the PV sources PV1 and PV2 respectively. These two values of modulation indices 'm_{a1}' and 'm_{a2}' individually controls the operating voltages of two PV sources or track MPP for two PV sources individually. Further, the two modulation indices 'm_{a1}' and 'm_{a2}' values are again used by the decoupled PWM technique for the determination of common frequency of the modulating wave. In decoupled PWM technique, the reference output voltage vectors of both the inverters are added. This may also help in increasing the operating voltage range for the PV array. Also, the usage of decoupled PWM technique with OEWIM gives the option of using two sets of PV arrays with low PV/dc-bus voltage [46]. This reduces the voltage rating of dc-bus capacitor and semiconductor devices. As the system uses independently two individual sets of PV array configurations, this helps in minimizing the shading problem. This can be supported by the usage of two independent MPPT algorithms for the two sets of PV array. Thus, the proposed system also facilitates the usage of different combinations of modules or groups for the two sets of PV array. In other words, it distributes the MPPT between the two sets of PV array configuration where each source tracks MPP individually. Thus, dual/distributed MPPT algorithm ensures the maximum utilization of both the PV arrays. The maximum power extracted by using individual MPPT algorithm, is then given to the motor-pump set via a dual-inverter.

In addition to the decoupled PWM technique, the usage of simple V/f control strategy in motor control, further ensures the high performance of OEWIM-pump set. This can be attributed to the fact that V/f control maintains the rated flux which helps in retaining the rated torque capability of the motor. Thus, it effectively utilizes the PV power by maintaining optimum torque with respect to power generated at the PV sources. Details of the implementation of dual MPPT algorithm along with the inverter and motor control technique is described below.

The simple and robust Perturb and Observe (P and O) algorithm was employed in the proposed system to extract the maximum possible power from both the PV sources (see Fig. 4). The proposed system consists of two sets of PV arrays and each array is connected to an individual MPPT controller namely MPPT1 and MPPT2 as shown in Fig. 2. The dual MPPT algorithm modifies or decide the corresponding modulation index ('m_{a1}' and 'm_{a2}') for the isolated dual-inverter. The algorithm requires the average value of voltages and currents of the two PV sources employed in the system. Thus, the algorithm first senses the average value of the PV voltages (V_{pv1}), (V_{pv2}), and currents (I_{pv1}), (I_{pv2}) from two sets of PV arrays PV1 and PV2 respectively. Then the individual PV power 'P_{pv1}' and 'P_{pv2}' for PV arrays PV1 and PV2 respectively are calculated. The calculated individual PV power and sensed voltage are then compared with their previous values for determining the sign of the slope of the p–v curve for both the PV sources separately. With respect to the sign of the slope (+ve or −ve) the values of modulation indices 'm_{a1}' and 'm_{a2}' are modified (decreased or increased) by a small constant value (Δm_a). The modified values of modulation indices 'm_{a1}' and 'm_{a2}' for the individual inverters are further processed with the operating voltage of the PV array for the calculation of resultant reference phase output voltage vector '$\vec{V}_{sr}$' as

given in (20). This is done because, the value of PV operating voltages for both the sources are not equal and constant. So, the effect of change in 'V_{pv1}' and 'V_{pv2}' together could be taken care by the algorithm to get effective tracking of maximum power. Further, as the decoupled PWM is employed, the resultant three-phase voltage vector across the windings of the motor is the sum of the two vectors 'OP$_1$' and 'O$\dot{}$P$_2$' (Fig. 2) as given below,

$$|\vec{V}_{sr}| = (m_{a1} \times V_{pv1} + m_{a2} \times V_{pv2}) = |\vec{V}_{sr1}| + |\vec{V}_{sr2}| \qquad (20)$$

Thus, the challenge associated with the operation of single-stage system with dual MPPT along with the motor control is solved with the consideration of resultant vector. In other words, the problem of common modulating frequency for both the inverters can be resolved by using '$\vec{V}_{sr}$' in calculating 'f_{mod}' for both inverters as described below.

$$f_{\mathrm{mod}} = \frac{|\vec{V}_{sr}| \times f_{rated}}{|\vec{V}_{sr(rated)}|} \qquad (21)$$

where '$\vec{V}_{sr(rated)}$' is the maximum output phase voltage of the OEWIM operating in the linear modulation region and 'f_{rated}' is the frequency of the rated voltage at rated power output in the linear modulation region. For a peak phase voltage of 325 V, from the dual-inverter configuration system, $\vec{V}_{sr(rated)}$ is calculated as follows:

$$\vec{V}_{sr(rated)} = \left(\frac{\sqrt{3}}{2}\right) \times V_{dc} = \left(\frac{\sqrt{3}}{2}\right) \times 564 \approx 488 \text{ V} \qquad (22)$$

where 564 V is the total required PV/dc-bus voltage to maintain the peak phase voltage of 325 V in the linear modulation range for the proposed PWM technique. So, to implement the V/f control for the proposed system the modulating frequency 'f_{mod}' is calculated using (21) and (22). The calculated value of 'f_{mod}' is then used by the decoupled PWM algorithm of the individual inverters for the generation of required PWM pulses. The position angle 'α' (see Figs. 2 and 4) of the output voltage vector for Inverter-1 and Inverter-2 is calculated based on 'f_{mod}' and sampling time period, 'T_s'. Decoupled PWM then uses the reference voltage space vector '$|V_{sr}|\angle\alpha$' that is to be synthesized from the electrically isolated dual-inverter system. This vector '$|V_{sr}|\angle\alpha$' is resolved into two opposite components '$|V_{sr1}|\angle\alpha$' (OP1 in Fig. 2) and '$|V_{sr2}|\angle(180° + \alpha)$' (O'P2 in Fig. 2). The decoupled components OP1 and O'P2 are then given as the reference voltage vectors for Inverter-1 and Inverter-2 respectively. These vectors are then used by the carrier based space vector PWM technique [47] to generate the required gating pulses for the power semiconductor devices of the dual-inverter.

4. Simulation results

To study the performance of the proposed system operated with dual MPPT, simulation is performed using MATLAB/Simulink software. The simulation is done using the 48 samples per cycle of the applied fundamental phase voltage irrespective of the magnitude of the resultant three-phase voltage vector across the windings of the motor 'V_{sr}'. Specifications considered in the simulation for the PV system and the OEWIM motor are given in Table 1. To verify the performance of the dual MPPT algorithm, asymmetrical configurations for the two PV arrays (PV1 and PV2) are considered as indicated in Table 1. Also, to study the dynamic behavior of the system, four different environmental conditions were considered. Fig. 5(a) and (b) show the insolation and temperature respectively at which both the PV arrays are operated. Also, it can be observed from subplots (c) and (d) of Fig. 5 that the value of PV current increases with the corresponding decrease in its voltage. This
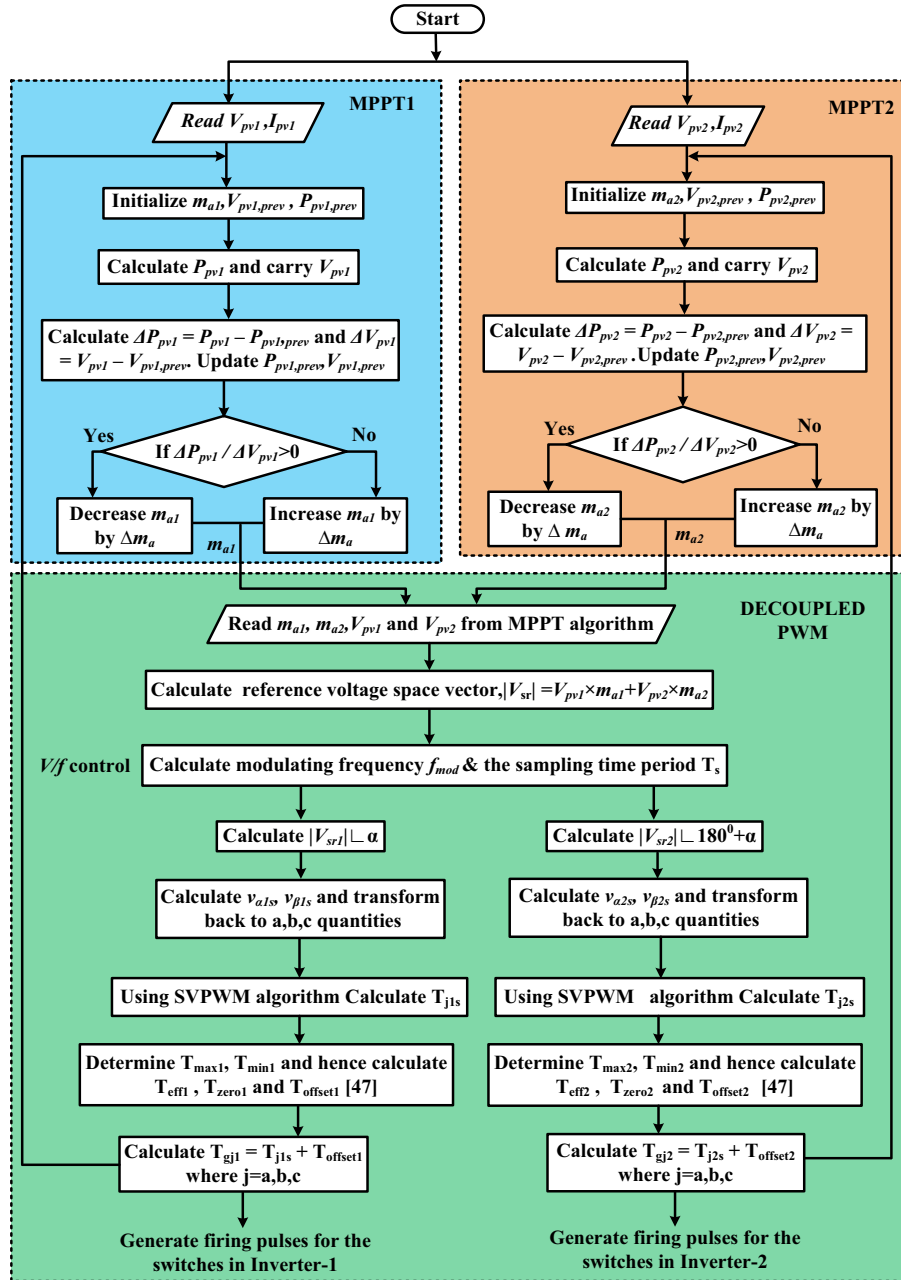
Fig. 4. Flow chart of the dual MPPT and decoupled PWM algorithm used in the proposed system.

Table 1
Parameters of solar PV system and OEWIM.

PV module@ STC [44]		OEWIM	
V_{oc}	21.0 V	Rated voltage(L–L) and power	400V, 4 kW
I_{sc}	3.74 A	Rated speed, Nr	1430 rpm
V_{MPP}	17.1 V	Stator winding resistance, r_s	1.405 Ω
I_{MPP}	3.5 A	Leakage reactance, $x_{ls} = x_{lr}$	1.8344 Ω
P_{MPP}	59.9 W	Supply frequency, f	50 Hz
PV1 array	22 × 2	No. of poles, P	4
PV2 array	11 × 2	Rotor winding resistance, r_r	1.395 Ω

nearly confirms the PV array characteristics. Another observation is that by changing the insolation (G) and temperature (T), there is corresponding change in the PV variables like current and voltage of both the PV arrays. Furthermore, it can be observed from the simulation results shown in Fig. 5 that modulation indices 'm_{a1}'

and 'm_{a2}' for the individual inverter (Inverter-1 and Inverter-2) follows the respective PV power generated. Lower the value of PV power, lower is the value of respective modulation index 'm_{ah}'(where $h \in (1,2)$) at MPP, and vice versa. Thus, an increase or decrease in PV power leads to the respective increase or decrease in the value of corresponding modulation index 'm_{ah}'. This justifies that modulation indices 'm_{a1}' and 'm_{a2}'controls or tracks MPP for the two PV sources individually. This can be observed from simulation results in subplots (e) and (f) of Fig. 5.

Another useful observation from Fig. 5 is that the operating voltage of PV arrays passes through optimum (MPP) voltage for every step increase in insolation and temperature. Also, the small oscillations in modulation indices ('m_{a1}' and 'm_{a2}') clearly indicate operation of both the PV sources near MPP. This can also be concluded by the matching values of peak power during transient tracking and steady-state near MPP as given in the PV power
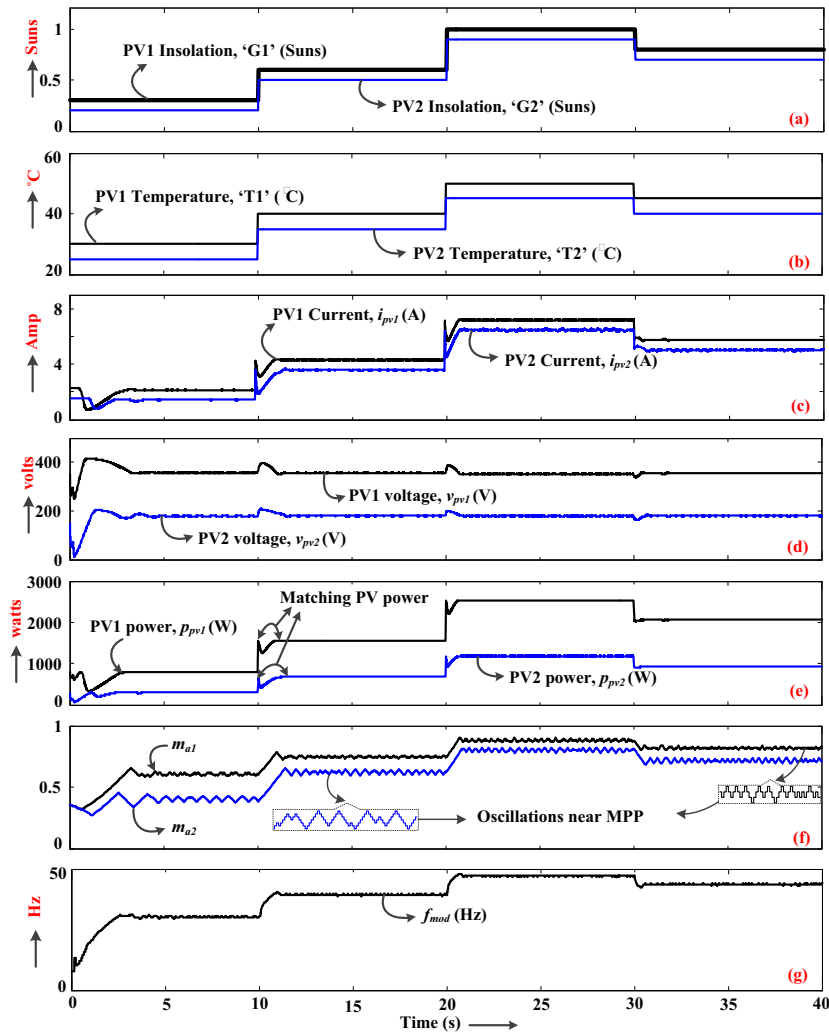
Fig. 5. Simulation results for the proposed system showing waveforms at PV source side.

subplot (e) of Fig. 5. Low ripple content in PV power and matching with peak PV power at transient and steady-state for both arrays confirms the effectiveness of the dual MPPT algorithm. Further, it can be noted that PV voltage waveform shows a sudden rise or fall in its value during the step increase or decrease in insolation and temperature. This can be attributed to charging and discharging of PV capacitor 'C_{PV}' with excess or deficit PV power during transient condition. Last subplot of Fig. 5 shows the waveform for the magnitude of modulating frequency, 'f_{mod}'. Effect of oscillations and increase or decrease in value of modulation indices ('m_{a1}' and 'm_{a2}') can be observed in the magnitude of modulating frequency 'f_{mod}'. Also, the time interval between the change in the values of modulation indices ('m_{a1}' and 'm_{a2}') increases with the decrease in the value of 'f_{mod}'. This can be attributed to synchronization of MPPT with V/f control.

Fig. 6 show the simulation results for motor-side parameters at four different environmental conditions as shown in subplots (a) and (b) of Fig. 5. Variations in the peak value of the motor phase voltage can be observed in subplot (a) of Fig. 6. This is mainly due to the corresponding variations in the resultant PV array voltage. The voltage of each individual PV sources with their corresponding modulation index defines the reference voltage vector 'V_{sr1}' and 'V_{sr2}' for Inverter-1 and Inverter-2 respectively as shown in subplot (b). The other plot in (b) is of 'V_{sr}' which is the resultant of 'V_{sr1}' and 'V_{sr2}'. The magnitude of the output reference voltage vector for each inverter defines the power contribution of the

respective PV source. Thus, an increase or decrease in the value of inverter reference voltage vector will lead to respective increase or decrease in the corresponding PV power. This can be verified with subplots (e) of Fig. 5 and (b) of Fig. 6. Further, an interesting observation is that the nature of 'f_{mod}' (subplot (g) of Fig. 5) and 'V_{sr}' (subplot (b) of Fig. 6) waveforms is same. This can also be attributed to the working of V/f control strategy.

The OEWIM is coupled to centrifugal water pump load, where developed torque and output power are directly proportional to square and cube of the motor speed respectively. Thus, any change in the motor speed will directly affect the motor torque and the output power. If the system performs effectively then change in PV power should be reflected on the speed of the motor-pump. This can be verified from the subplot (e) of Fig. 5 and subplots (d), (e) and (f) of Fig. 6. This can also be observed from the peak value of the motor phase current. The value of motor phase current increases or decreases with respect to the torque requirements. Thus, an increase or decrease in the torque value results in corresponding increase or decrease in the phase current. Another way to measure the system performance is with respect to the slip value and slip power. The values of slip and slip power increases or decreases with the respective increase or decrease in the value of developed torque or generated PV power. This can be attributed to the fact that slip value is mainly controlled by developed torque. Increase in the value of developed torque will result in the corresponding increase in slip value and therefore the slip power. This
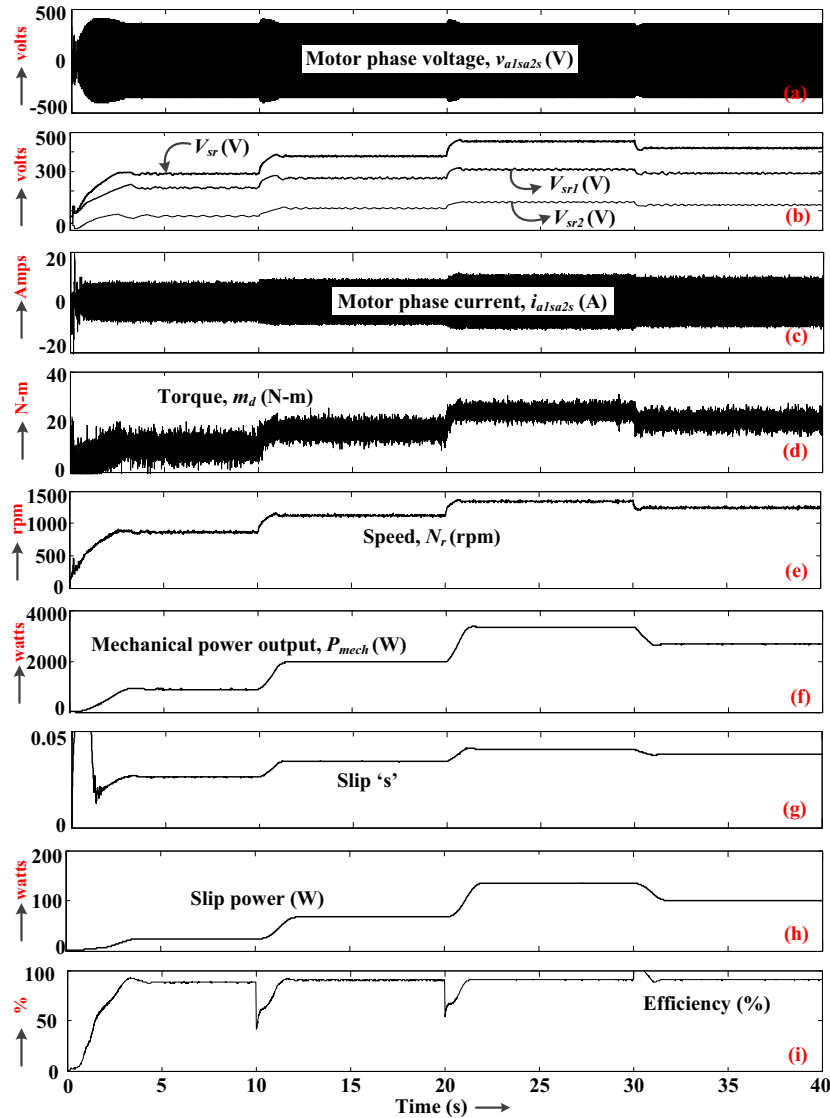
Fig. 6. Simulation results for the proposed system showing waveforms at motor-pump side.

can also be observed in Table 2 which summarizes the simulation results obtained at four different environmental conditions. Highest value of slip near rated PV power is 4.00% as given in Table 2. Low value of slip (below 5%) as can be observed from subplot (g) of Fig. 6 confirms the high performance of the motor with low slip power losses. Last subplot of Fig. 6 show the efficiency curve of motor power with respect to the input PV power. At steady state, efficiency of the motor is near to 90% for various environmental conditions as can be observed from Table 2.

Fig. 7 shows the expanded view of the motor phase voltage and current waveform from the subplots (a) and (c) of Fig. 6 respec-

tively. More than three-level operation can easily be observed in the waveform of the motor phase voltage. This helps in reducing the current ripple and improves the THD of the current waveform compared to three-level operation. Diminution in phase current ripple helps in reducing the torque and power ripple and which in turn improves the motor performance. High magnitude of ripple content in the current waveform at lower insolation can be attributed to larger magnitude of high frequency harmonics in the Fast Fourier Transform (FFT) plot of the phase voltage. This can be observed from FFT plots of the motor phase current and voltage in Fig. 7. It can also be observed that the THD of the phase voltage improves with increase in the value of modulating frequency 'f_{mod}' or output power. Thus, the magnitude of ripple content and the THD value in current waveform decreases with the increase in modulating frequency 'f_{mod}' or output power.

5. Conclusion

The solution for two independent PV source fed OEWIM for water-pump load is presented in this paper. The proposed system is operated using dual MPPT algorithm where the maximum power from both the sources are extracted separately. This improves the

Table 2
Summary of simulation results for the proposed system.

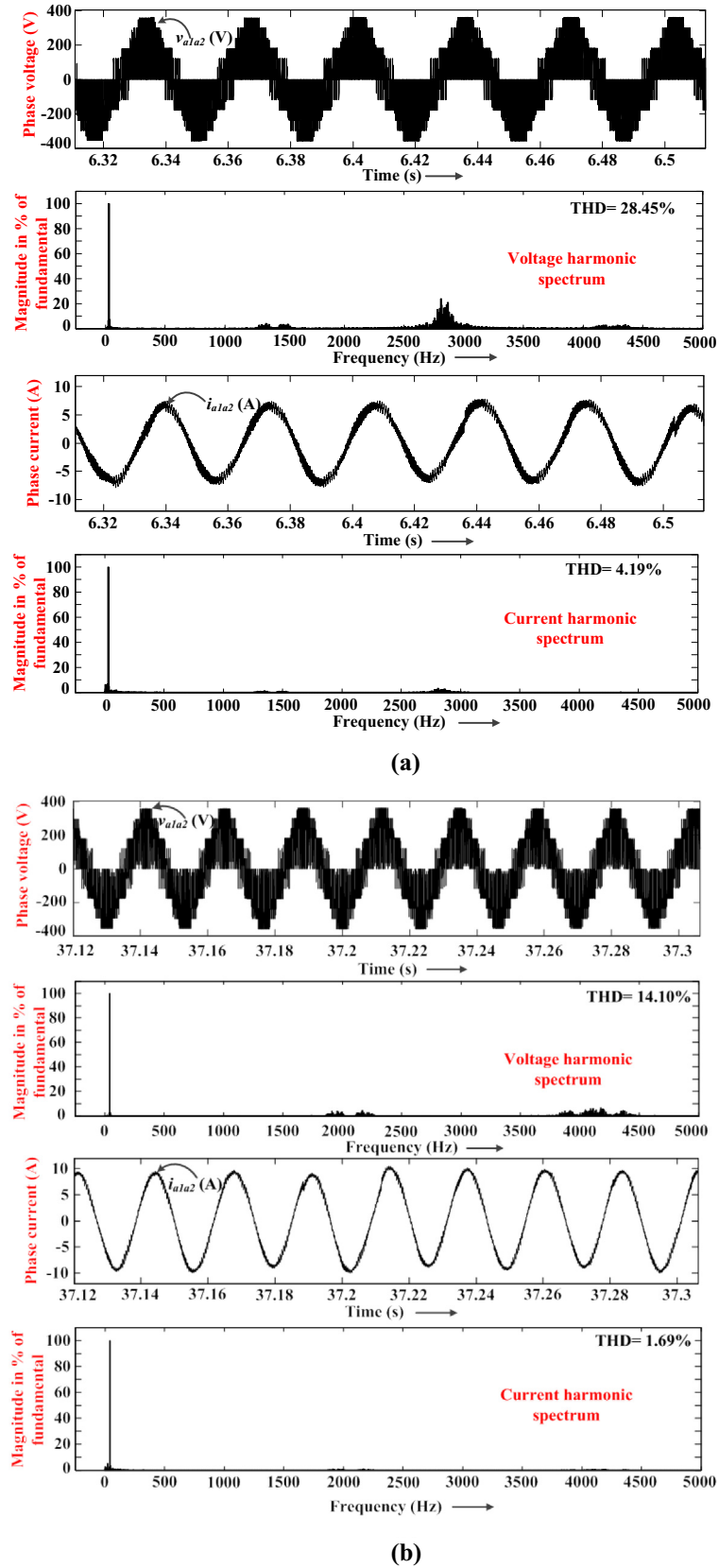| G1 (Suns)/ T1 (°C)	G2 (Suns)/ T2 (°C)	PV Power (W)	η (%)	Speed (rpm)	Torque (N-m)	Slip (%)	Slip Power (W)
0.3/30	0.2/25	1018	87.85	863.00	09.90	2.61	23.35
0.6/40	0.5/35	2176	90.16	1121.75	16.70	3.41	66.88
0.8/45	0.7/40	2941	90.29	1241.00	20.43	3.79	100.60
1.0/50	0.9/40	3686	90.26	1338.40	23.74	4.00	134.40

Fig. 7. Motor phase voltage (v_{a1a2}) and current (i_{a1a2}) with their FFT plot at steady state (a) at low insolation and (b) at high insolation condition.

performance of the PV water pumping system, since, maximum power can be extracted effectively from both the PV sources. In addition, the operation at low value of the slip using V/*f* control justifies efficient operation of the motor. High performance of the system for different values of insolation and temperature can be observed in Table 2. Another advantage of the proposed system is it gives more

than three-levels in the phase voltage for asymmetrical configuration with ratio of 2:1 dc-bus voltages for the two PV sources of the OEWIM. This reduces the motor torque ripple content. Thus, it improves the performance of the system. Therefore, a high performance water-pump solution is proposed which utilizes both the PV source and the motor efficiently. The given solution can also be extended for multiple PV sources as given in Fig. 1(e).

References

[1] Kamel Barra, Djamel Rahem, Predictive direct power control for photovoltaic grid connected system: an approach based on multilevel converters, Energy Convers. Manage. 78 (2014) 825–834.

[2] Kamal Himour, Kaci Ghedamsi, El Madjid Berkouk, Supervision and control of grid connected PV-Storage systems with the five level diode clamped inverter, Energy Convers. Manage. 77 (2014) 98–107.

[3] Necmi Altin, Saban Ozdemir, Three-phase three-level grid interactive inverter with fuzzy logic based maximum power point tracking controller, Energy Convers. Manage. 69 (2013) 17–26.

[4] S. Lalouni, D. Rekioua, T. Rekioua, E. Matagne, Fuzzy logic control of stand-alone photovoltaic system with battery storage, in: J. Power Sources 193 (2009) 899–907.

[5] Tamer Khatib, Ibrahim A. Ibrahim, Azah Mohamed, A review on sizing methodologies of photovoltaic array and storage battery in a standalone photovoltaic system, Energy Convers. Manage. 120 (2016) 430–448.

[6] P.E. Campana, H. Li, J. Zhang, R. Zhang, J. Liu, J. Yan, Economic optimization of photovoltaic water pumping systems for irrigation, Energy Convers. Manage. 95 (2015) 32–41.

[7] Ceyda Olcan, Multi-objective analytical model for optimal sizing of stand-alone photovoltaic water pumping systems, Energy Convers. Manage. 100 (2015) 358–369.

[8] Belkacem Bouzidi, New sizing method of PV water pumping systems, Sustainable Energy Technol. Assess. 4 (2013) 1–10.

[9] Yahia Bakelli, Amar Hadj Arab, Boubekeur Azoui, Optimal sizing of photovoltaic pumping system with water tank storage using LPSP concept, Sol. Energy 85 (2011) 288–294.

[10] Abdelmalek Mokeddem, Abdelhamid Midoun, D. Kadri, Said Hiadsi, Iftikhar A. Raja, Performance of a directly-coupled PV water pumping system, Energy Convers. Manage. 52 (2011) 3089–3095.

[11] J. Appelbaum, Starting and steady-state characteristics of dc-motors powered by solar cell generators, IEEE Trans. Energy Convers. 1 (1986) 17–25.

[12] A. Boutelhig, Y. Bakelli, I. Hadj Mahammeda, A. Hadj Arab, Performances study of different PV powered DC pump configurations for an optimum energy rating at different heads under the outdoor conditions of a desert area, Energy 39 (2012) 33–39.

[13] Ahmed M. Kassem, MPPT control design and performance improvements of a PV generator powered DC motor-pump system based on artificial neural networks, Electr. Power Energy Syst. 43 (2012) 90–98.

[14] S.S. Chandel, M. Nagaraju Naik, Rahul Chandel, Review of solar photovoltaic water pumping system technology for irrigation and community drinking water supplies, in: Renewable Sustainable Energy Rev. 49 (2015) 1084–1099.

[15] A. Terki, A. Moussi, A. Betka, N. Terki, An improved efficiency of fuzzy logic control of PMBLDC for PV pumping system, Appl. Math. Model. 36 (2012) 934–944.

[16] S.A.KH. Mozaffari Niapour, S. Danyali, M.B.B. Sharifian, M.R. Feyzi, Brushless DC motor drives supplied by PV power system based on Z-source inverter and FL-IC MPPT controller, in: Energy Convers. Manage. 52 (2011) 3043–3059.

[17] Vilas R. Vimal Chand Sontake, Kalamkar, Solar photovoltaic water pumping system – a comprehensive review, in: Renewable Sustainable Energy Rev. 59 (2016) 1038–1067.

[18] Kamlesh Yadav, O.S. Sastry, R. Wandhare, N. Sheth, M. Kumar, B. Bora, Rashmi Singh, Renu, A. Kumar, Performance comparison of controllers for solar PV water pumping applications, Sol. Energy 119 (2015) 195–202.

[19] D. Mezghanni, R. Andoulsi, A. Mami, G. Dauphin-Tanguy, Bond graph modelling of a photovoltaic system feeding an induction motor-pump, Simul. Model. Pract. Theory 15 (2007) 1224–1238.

[20] S.R. Bhat, A. Pittet, B.S. Sonde, Performance optimization of induction motor-pump system using photovoltaic energy source, IEEE Trans. Ind. Appl. 23 (1987) 995–1000.

[21] M.N. Eskander, A.M. Zaki, A maximum efficiency photovoltaic induction motor pump system, J. Renewable Energy 10 (1997) 53–60.

[22] J.V.M. Caracas, G. Farias, L. Teixeira, L. Ribeiro, Implementation of a high-efficiency, high-lifetime and low-cost converter for an autonomous photovoltaic water pumping system, IEEE Trans. Ind. Appl. 50 (2014) 631–641.

[23] Chergui Moulay-Idriss, Bourahla Mohamed, Application of the DTC control in the photovoltaic pumping system, Energy Convers. Manage. 65 (2013) 655–662.

[24] Y. Yao, P. Bustamante, R.S. Ramshaw, Improvement of induction motor drive systems supplied by photovoltaic arrays with frequency control, IEEE Trans. Energy Convers. 9 (1994) 256–262.

[25] T.P. Corrêa, S.I. Seleme Jr., S.R. Silva, Efficiency optimization in stand-alone photovoltaic pumping system, J. Renewable Energy 41 (2012) 220–226.

[26] S. Jain, A.K. Thopukara, R. Karampuri, V.T. Somasekhar, A single-stage photovoltaic system for a dual-inverter-fed open-end winding induction motor drive for pumping applications, IEEE Trans. Power Electron. 30 (2015) 4809–4818.

[27] S. Jain, R. Karampuri, V.T. Somasekhar, An integrated control algorithm for a single-stage PV pumping system using an open-end winding induction motor, IEEE Trans. Ind. Electron. 63 (2016) 956–996.

[28] Saban Ozdemir, Necmi Altin, Ibrahim Sefa, Single stage three level grid interactive MPPT inverter for PV systems, Energy Convers. Manage. 80 (2014) 561–572.

[29] G. Grandi, P. Sanjeevikumar, Y. Gritli, F. Filippetti, Experimental investigation of fault-tolerant control strategies for quad-inverter converters, Conf. Proc. IEEE Intl. Conf. on Electrical System for Aircraft, Railway and Ship Propulsion, IEEE-ESARS'12, Bologna (Italy), 2012, pp. 1–8. 16-18 Oct.

[30] G. Grandi, P. Sanjeevikumar, Y. Gritli, F. Filippetti, Fault-tolerant control strategies for quad-inverter induction motor drives with one failed inverter, in: Conf. Proc. IEEE 20th Intl. Conf. On Electrical Machines, IEEE-ICEM'12, Marseille (France), 2012, pp. 957–964. 2–5 Sept.

[31] G. Grandi, P. Sanjeevikumar, D. Casadei, Preliminary hardware implementation of a six-phase quad-inverter induction motor drive, in: Conf. Proc. The 14th IEEE European Power Electron. And Appl., IEEE-EPE'11, Birmingham (United Kingdom), 2011, pp. 1–9. 30 Aug.-1 Sept.

[32] G. Grandi, P. Sanjeevikumar, D. Ostojic, C. Rossi, Quad-inverter configuration for multi-phase multi-level ac motor drives, in: Conf. Proc., Intl. Conf. Computational Technologies in Elect. And Electron. Engg., IEEE-SIBIRCON'10, Irkutsk Listvyanka (Russia), 2010, pp. 631–638. 11-15 Jul.

[33] P. Sanjeevikumar, G. Grandi, Frede Blaabjerg, Patrick Wheeler, Olorunfemi Ojo, Analysis and implementation of power management and control strategy for six-phase multilevel AC drive system in fault condition, Eng. Sci. Technol. Int. J. 19 (1) (2016) 31–39.

[34] P. Sanjeevikumar, G. Grandi, Olorunfemi Ojo, Frede Blaabjerg, Direct vector controlled six-phase asymmetrical induction motor with power balanced space vector PWM multilevel operation, in: International Journal of Power and Energy Conversion, vol. 7, Inderscience Publications, 2016, pp. 57–83. No. 1.

[35] P. Sanjeevikumar, G. Grandi, Frede Blaabjerg, Olorunfemi Ojo, Patrick Wheeler, Power sharing algorithm for vector controlled six-phase AC motor with four customary three-phase voltage source inverter drive, in: Engineering Science and Technology: An International Journal (JESTECH), vol. 19, Elsevier Journal Publications, 2016, pp. 31–39. No. 1.

[36] Yang Du, Dylan Dah-Chuan Lu, Battery-integrated boost converter utilizing distributed MPPT configuration for photovoltaic systems, Sol. Energy 85 (2011) 1992–2002.

[37] J. Solórzano, M.A. Egido, Automatic fault diagnosis in PV systems with distributed MPPT, Energy Convers. Manage. 6 (2013) 925–934.

[38] J. Solórzano, M.A. Egido, Hot-spot mitigation in PV arrays with distributed MPPT (DMPPT), in: Sol. Energy 101 (2014) 131–137.

[39] M. Muthuramalingam, P.S. Manoharan, Comparative analysis of distributed MPPT controllers for partially shaded stand alone photovoltaic systems, Energy Convers. Manage. 86 (2014) 286–299.

[40] Marco Balato, Massimo Vitelli, A new control strategy for the optimization of Distributed MPPT in PV applications, Electr. Power Energy Syst. 62 (2014) 763–773.

[41] Rosario. Carbone, PV plants with distributed MPPT founded on batteries, Sol. Energy 122 (2015) 910–923.

[42] V. Sonti, S. Jain, S. Bhattacharya, Analysis of Modulation Strategy for the Minimization of Leakage Current in the PV Grid Connected Cascaded Multi-Level Inverter, accepted for publication in IEEE Trans. Power Electron.

[43] B. Venugopal Reddy, V.T. Somasekhar, Y. Kalyan, Decoupled space-vector PWM strategies for a four-level asymmetrical open-end winding induction motor drive with waveform symmetries, IEEE Trans. Ind. Electron. 58 (2011) 5130–5141.

[44] G. Walker, Evaluating MPPT converter topologies using a MATLAB PV model, J. Elect. Eng. 21 (2001) 49–56.

[45] H. Stemmler, P. Guggenbach, Configurations of high-power voltage source inverter drives, Proc. EPEA (1993) 7–12.

[46] V.T. Somasekhar, E.G. Shivakumar, K. Gopakumar, A multi level voltage space phasor generation for an open-end winding induction motor drive using a dual inverter scheme with asymmetrical DC-link voltages, J. Eur. Power Electron. 12 (2002) 59–77.

[47] Dae-Woong Chung, Joohn-Sheok Kim, Seung-Ki Sul, Unified voltage modulation technique for real-time three-phase power conversion, IEEE Trans. Ind. Appl. 34 (1998) 374–380.